Rock and Soil Mechanics

Volume 41 | Issue 6 Article 2

11-11-2020

Experimental study on surrounding rock deformation and acoustic emission characteristics of rectangular roadway under different loads

Gong-yu HOU
School of Mining Engineering and Geology, Xinjiang Institute of Engineering, Urumqi, Xinjiang 830091, China

Hao-yong JING
School of Mechanics and Civil Engineering, China University of Mining and Technology (Beijing), Beijing 100083, China, jinghaoyong@126.com

Jin-ping LIANG
School of Mechanics and Civil Engineering, China University of Mining and Technology (Beijing), Beijing 100083, China

Jin-xin TAN
School of Mechanics and Civil Engineering, China University of Mining and Technology (Beijing), Beijing 100083, China

See next page for additional authors

Custom Citation

HOU Gong-yu, JING Hao-yong, LIANG Jin-ping, TAN Jin-xin, ZHANG Yong-kang, YANG Xi, XIE Xin, . Experimental study on surrounding rock deformation and acoustic emission characteristics of rectangular roadway under different loads[J]. Rock and Soil Mechanics, 2020, 41(6): 1818-1828.

Experimental study on surrounding rock deformation and acoustic emission characteristics of rectangular roadway under different loads

Authors

Gong-yu HOU, Hao-yong JING, Jin-ping LIANG, Jin-xin TAN, Yong-kang ZHANG, Xi YANG, and Xin XIE

Rock and Soil Mechanics 2020 41(6): 1818−1828 ISSN 1000−7598
https: //doi.org/10.16285/j.rsm.2019.5931 rocksoilmech.researchcommons.org/journal

Experimental study on surrounding rock deformation and acoustic emission characteristics of rectangular roadway under different loads

HOU Gong-yu[1, 2], JING Hao-yong[1], LIANG Jin-ping[1], TAN Jin-xin[1], ZHANG Yong-kang[1], YANG Xi[1], XIE Xin[1]

1. School of Mechanics and Civil Engineering, China University of Mining and Technology (Beijing), Beijing 100083, China
2. School of Mining Engineering and Geology, Xinjiang Institute of Engineering, Urumqi, Xinjiang 830091, China

Abstract: To investigate the unloading deformation, failure and acoustic emission characteristics during excavation of rectangular roadway under different initial geostresses, excavation unloading model tests were carried out on casted surrounding-rock specimens made of cement mortar. The deformation and failure characteristics of the roof, corner and surrounding rock as well as the evolution characteristics of AE impact count, damage variable and frequency spectrum were obtained. Experimental results showed that: 1) The failure of rectangular roadway was mainly caused by the radial tension strain of the roof and surrounding rock, and the tangential compression strain of the corner. The deformation characteristics of the surrounding rock at the roof were similar to that at the side wall. 2) Increase of the initial geostress had significant effect on the radial strain rate of the roof (or the side wall) and the tangential strain rate of the corner while not significant on others. 3) The evolution characteristics of AE impact count and damage variable revealed the phased failure process of surrounding rock from micro-fracture initiation, expansion to macro-crack development until the occurrence of main fracture. The time of main fracture occurring may be relatively delayed as the geostress increased, and the relative damage proportion after excavation unloading increased nonlinearly with the increase of the initial geostress. 4) The phenomenon that the peak frequency of AE signal was concentrated with gradually increased amplitude could be regarded as a precursor information of the main fracture occurring in the surrounding rock. The higher the initial geostress, the wider the distribution of the peak frequency concentrated section. 5) As the initial geostress increased, the inner wall of surrounding rock specimens demonstrated the evolution of damage from micro-cracks to abscission layer, and to block fracture of rock mass. The failure modes of rock mass were dominated by the tensile heave in the roof and side wall, and accompanied by the phenomenon of delamination and fragmentation. Furthermore, compression and shear failure were observed at the corner when the specimens lost the bearing capacity.

Keywords: initial geostress; rectangular roadway; excavation unloading; deformation failure; acoustic emission

1 Introduction

With the continuous emergence of deep mining engineering, rectangular roadways exhibit the advantages of convenient construction and high utilization rate. However, their ability to withstand lateral pressure is poor, and the cross-sectional shape will cause the effect of stress concentration to be increased. Therefore, it is of great theoretical significance and engineering application value to study the deformation law, failure characteristics and acoustic emission characteristics of surrounding rock during excavation and unloading of rectangular roadways under different initial geostresses.

A significant number of studies have shown that the excavation and unloading of roadway will lead to the redistribution of the surrounding rock stress, and will easily provoke the initiation and expansion of micro-cracks and macro-cracks[1−2]. Existing research mainly explored the deformation and failure characteristics and acoustic emission (AE) characteristics of surrounding rocks through triaxial loading and unloading tests. Based on the triaxial unloading test of rock, Qiu et al.[3] and Huang et al.[4] believed that the unloading rate would have a significant effect on the deformation and mechanical properties of the rock. Li et al.[5] obtained the strength changes and failure modes of different rocks in deep underground engineering. Su et al.[6] and Du et al.[7] discussed the different factors and energy changes that lead to rockburst during roadway excavation based on true triaxial loading and unloading tests of rock. In addition, the application of acoustic emission to the investigation of rock damage has also stimulated research into exploring its characteristics. The accumulated AE energy can better reflect the true energy of the AE event, which can be used to evaluate the energy release characteristics of rock during the entire destruction process[8]. Thomas et al.[9] obtained the evolution characteristics of rock damage and acoustic

Received: 23 May 2019 Revised: 31 October 2019
This work was supported by the General Program of National Natural Science Foundation of China(51574247).
First author: HOU Gong-yu, male, born in 1965, PhD Professor, PhD supervisor, mainly engaged in teaching and research work in geotechnical engineering and rock mechanics. E-mail: hgyht@126.com
Corresponding author: JING Hao-yong, male, born in 1993, Master candidate, majoring in and rock mechanics. E-mail: jinghaoyong@126.com

emission parameters during loading and unloading. The ordinary triaxial test can study some mechanical properties and deformation characteristics of rock, but it is difficult to show the true state of the roadway during excavation and unloading. Hou et al.[10] established an elastoplastic theory model of circular roadway with axisymmetric lanes. Although the theoretical analysis is clear in concept, due to the use of various assumptions, there is still a certain gap between the theory and the actual roadway excavation status.

In order to accurately study the deformation and failure mechanism of surrounding rock, a number of researchers have conducted laboratory tests simulating roadway excavation and unloading. For instance, Hou et al.[11] used plaster specimens to examine the deformation and failure mechanism of surrounding rock during excavation and unloading of circular roadways. Wang et al.[12] obtained the failure evolution characteristics of surrounding rock of coal roadway based on model test using similar material. Yang[13] and Wang et al.[14] used hollow cylindrical rock specimens to explore the evolution relationship between triaxial strength and deformation parameters.

At present, simulations of the excavation and unloading process of rectangular roadways are mostly theoretical solutions or numerical tests based on certain projects. The magnitudes of the in-situ stress are relatively close. In this paper, cement-mortar specimens of surrounding rock with rectangular holes are used. Using the model test system for excavation and unloading of roadway surrounding rock reported in the literature[15], the deformation law, destruction mechanism and acoustic emission characteristics of surrounding rock during excavation and unloading of rectangular roadway under different initial stresses are investigated. The advantage of this experimental study is that it adopts the form of unloading the inner cavity of the surrounding rock specimen. The simulation process of excavation and unloading is similar to the situation on site in terms of mechanics, which is consistent with the simplified mechanical model of the elastic-plastic solution of a circular roadway.

2 Test scheme

2.1 Material mechanical parameters and specimen preparation

In the process of preparing surrounding-rock specimens, the proportions, mechanical parameters and design dimensions of the cement mortar materials are detailed in literature[16]. According to the theory of rock mechanics, surrounding rock within the range of 3−5 times roadway radius will be affected by the excavation. To meet the theoretical boundary conditions and in combination with the regimes of the test equipment in laboratory and the aspect ratio range of the rectangular roadway in actual engineering, the dimensions of the surrounding-rock specimen with rectangular holes used in the excavation and unloading test are designed to have a height of 270 mm and an outer diameter of 200 mm, and inner center rectangle size is 40 mm×50 mm. The strain gauges are located in the center of the roof rock(A), corner rock(B), and middle of the side wall rock(C), as shown in Fig.1. Three sets of gauges are arranged from inside to outside. Each measuring point monitors the radial, axial and tangential strains. The manufacturing and curing of the mold as well as the precisely processed specimen of the surrounding rock are shown in Fig.2. For details of AE parameter setting and sensor arrangement, readers can refer to the published literature.[16]

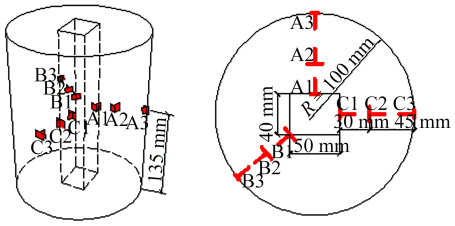

(a) Side view (b) Top view

Fig. 1 Strain gauges arrangement

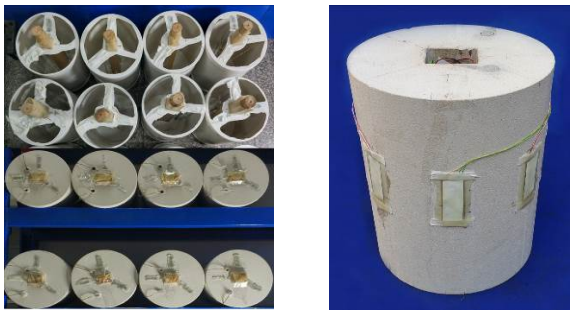

(a) Mould making and embryo casting (b) Precisely processed surrounding rock samples

Fig. 2 Manufacture and molding of specimens

2.2 Rectangular roadway excavation unloading model test system

The experiments adopt a small-scale model test system independently designed and developed by the research group for excavation and unloading of roadway surrounding rock[15], as shown in Fig.3. The system includes three subsystems, namely the loading and unloading subsystem, the acoustic emission monitoring subsystem, and the strain monitoring subsystem. When the surrounding-rock specimens under triaxial loading reach the initial in-situ stress, the axial and external cavity pressures are kept at a constant level, the internal

cavity load is removed to simulate the roadway excavation and unloading process. During the test, the monitoring of strain and acoustic emission is carried out simultaneously with the loading and unloading process. For details of AE parameter setting and sensor arrangement, readers are referred to the literature[16].

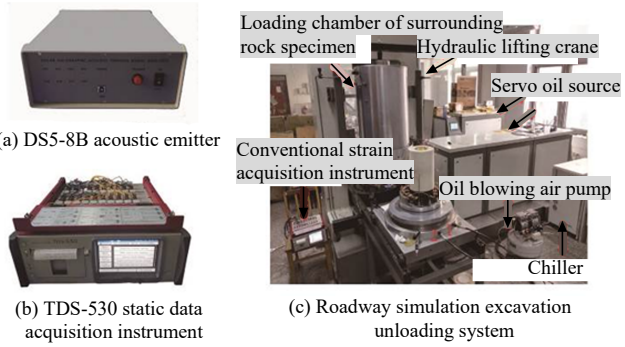

(a) DS5-8B acoustic emitter

(b) TDS-530 static data acquisition instrument

(c) Roadway simulation excavation unloading system

Fig. 3 Model testing system of roadway surrounding-rock under excavation unloading

2.3 Simulated excavation and unloading test

Roadway excavation and unloading refers to the process where the excavated body is removed under the stress of original rock, and the stress level inside the roadway (non-wall rock) is reduced from the originnal rock stress to zero. The stress on the surrounding rock specimen of rectangular roadway under excavation unloading during the experiment is shown in Fig.4. The distance from the center to the outer wall of the specimen is 5 times the excavation radius, which meets the boundary conditions of roadway excavation, so p_0 is the initial geostress (or original rock stress and in-situ stress). According to previous research on the elastoplastic theory of roadway excavation and unloading reported in the literatures[10, 17], the axial stress p_z equals to the original rock stress p_0 during the roadway excavation and unloading.

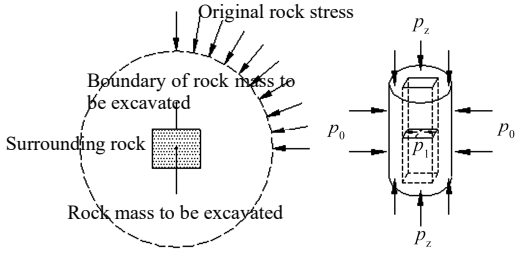

(a) Mechanical model of roadway excavation

(b) Initial stress exerted on surrounding rock specimen

Fig. 4 Mechanism model of rectangular roadway under excavation unloading

In the test, four different initial geostress levels of 10, 15, 20, and 30 MPa were set, of which 30 MPa was high initial geostress failure test, and only acoustic emission monitoring was performed. The specific test steps are as follows:

(1) In the loading stage, load the specimen to the predetermined initial in-situ stress level at a constant loading rate (0.1 MPa/s) in the directions of the three principal stresses (peripheral pressure p_0, internal confining pressure p_1, and axial pressure p_z).

(2) In the post-loading maintenance stage, the load was kept for 10 min so that the stress was evenly transmitted inside the surrounding rock specimen.

(3) In the unloading stage, the peripheral pressure p_0 and the axial pressure p_z were kept constant, and the inner confining pressure p_1 was removed at a rate of 0.05 MPa/s to simulate the excavation and unload ing process of the roadway.

(4) In the post-unloading maintenance stage, the three-dimensional stresses after the unloading was completed were kept constant for 15 minutes until the end of the test.

3 Strain analysis of surrounding rock

3.1 Strain-time evolution characteristics

The strain laws of the surrounding rock specimens under initial geostress of 10, 15, 20 MPa are shown in Fig.s 5 and 6. The post-stabilization period (60 s before unloading) was used as the zero point for recording the strain. The changes of the three-dimensional strain with time during excavation unloading and post-unloading maintenance were plotted, where the tensile strain is positive and compressive strain is negative. The comparison shows that the three-dimensional strain-time relationships of the surrounding rock specimens at the same measuring point are similar under different initial geostresses

3.1.1 Strain characteristics of surrounding rock at the roof and side-wall

The radial, tangential and axial strain laws of the roadway roof and the side-wall are similar (see Fig.5). The following analyses take the strain characteristics of each measurement point of the roof surrounding rock as an example.

(1) At the end of post-loading maintenance phase, the three-dimensional strain of each measuring point floated around the zero point, and the surrounding rock specimen was completely in the state of the corresponding initial geostress. Obvious tensile and compressive deformations have occurred at each measuring point since the start of unloading. As unloading progressed, the strain increased gradually. In the post-unloading maintenance phase, the surrounding rock continued to deform until gradually becoming stabilized. The higher the initial ground stress, the greater was the

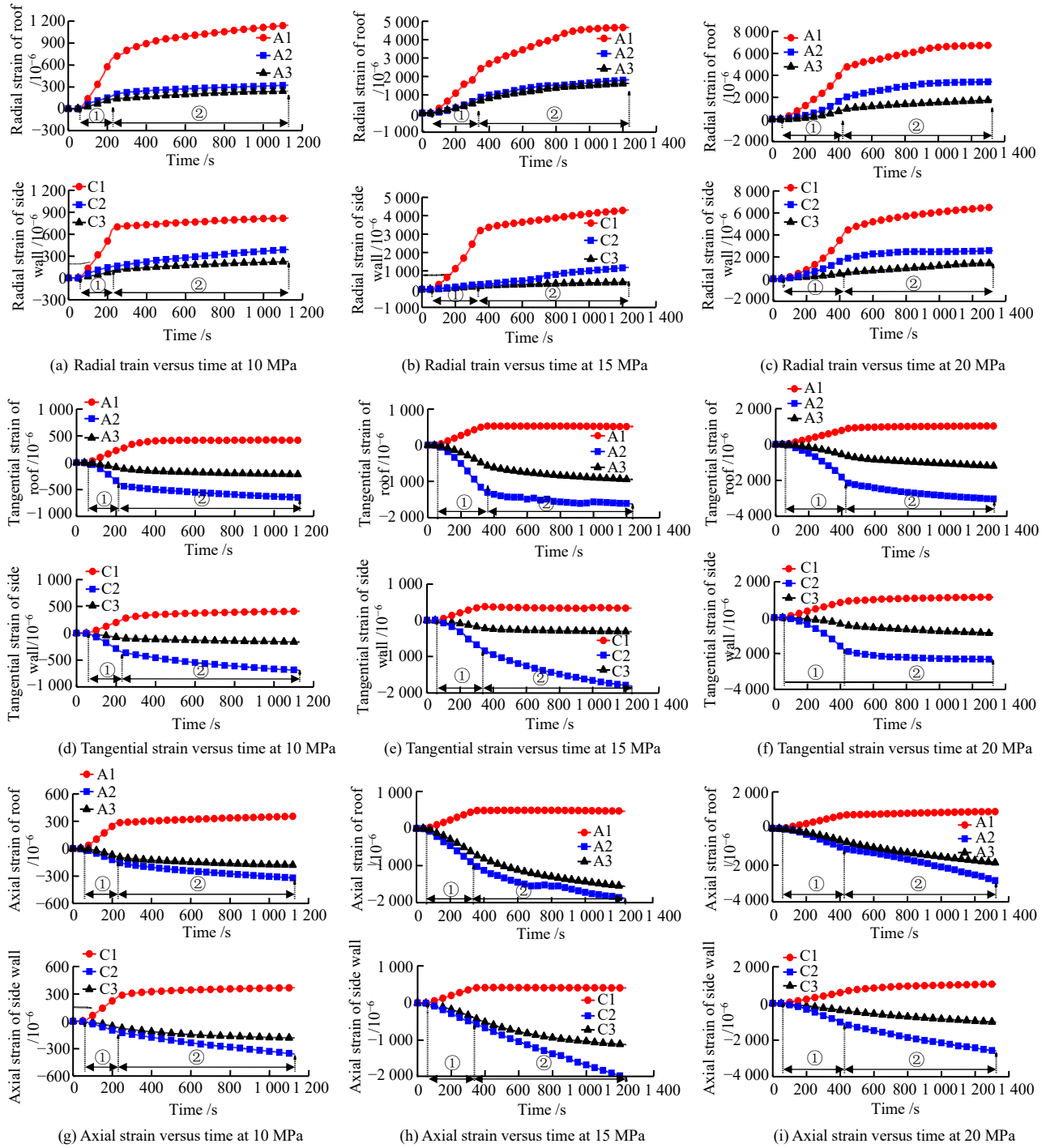

(a) Radial train versus time at 10 MPa (b) Radial train versus time at 15 MPa (c) Radial train versus time at 20 MPa

(d) Tangential strain versus time at 10 MPa (e) Tangential strain versus time at 15 MPa (f) Tangential strain versus time at 20 MPa

(g) Axial strain versus time at 10 MPa (h) Axial strain versus time at 15 MPa (i) Axial strain versus time at 20 MPa

Note: ① denotes the unloading stage; ② denotes the post-unloading maintenance stage.

Fig. 5 Strain characteristics of the surrounding rock at roof and side wall

deformation of the surrounding rock at the same measuring point.

(2) According to the three-dimensional strain characteristics of different measurement points, the strain law from the roof of the roadway to the deep surrounding rock can be inferred as follows: (i) Tensile strain occurs radially and reaches the largest amount around the periphery of the roadway, and the strain gradually decreases as progressing deeper into the surrounding rock. (ii) The tangential and axial strains are similar and surroundings of the roadway are all under tension. As the depth into surrounding rock increases, the stress gradually becomes compressive with a gradual decrease in deformation.

3.1.2 Strain characteristics of corner wall rock

The three-dimensional strain laws of the measuring points B1−B3 of the corner rock of the roadway are illustrated in Fig.6. The strain characteristics of measuring points are as follows:

(1) The tangential compressive strain at measuring point B1 is the largest at any time, followed by the radial tensile strain, so the tangential compressive

deformation mainly occurs around the corner of the roadway.

(2) The three-dimensional deformation laws from the corner of the roadway to the deeper surrounding rock are as follows: (i) The surrounding rock is under radial tension; the amount of deformation gradually decreases with depth. (ii) The tangential compression also causes the amount of deformation to gradually decrease. (iii) The characteristic of compressive strain is shown along the axial direction of each measuring

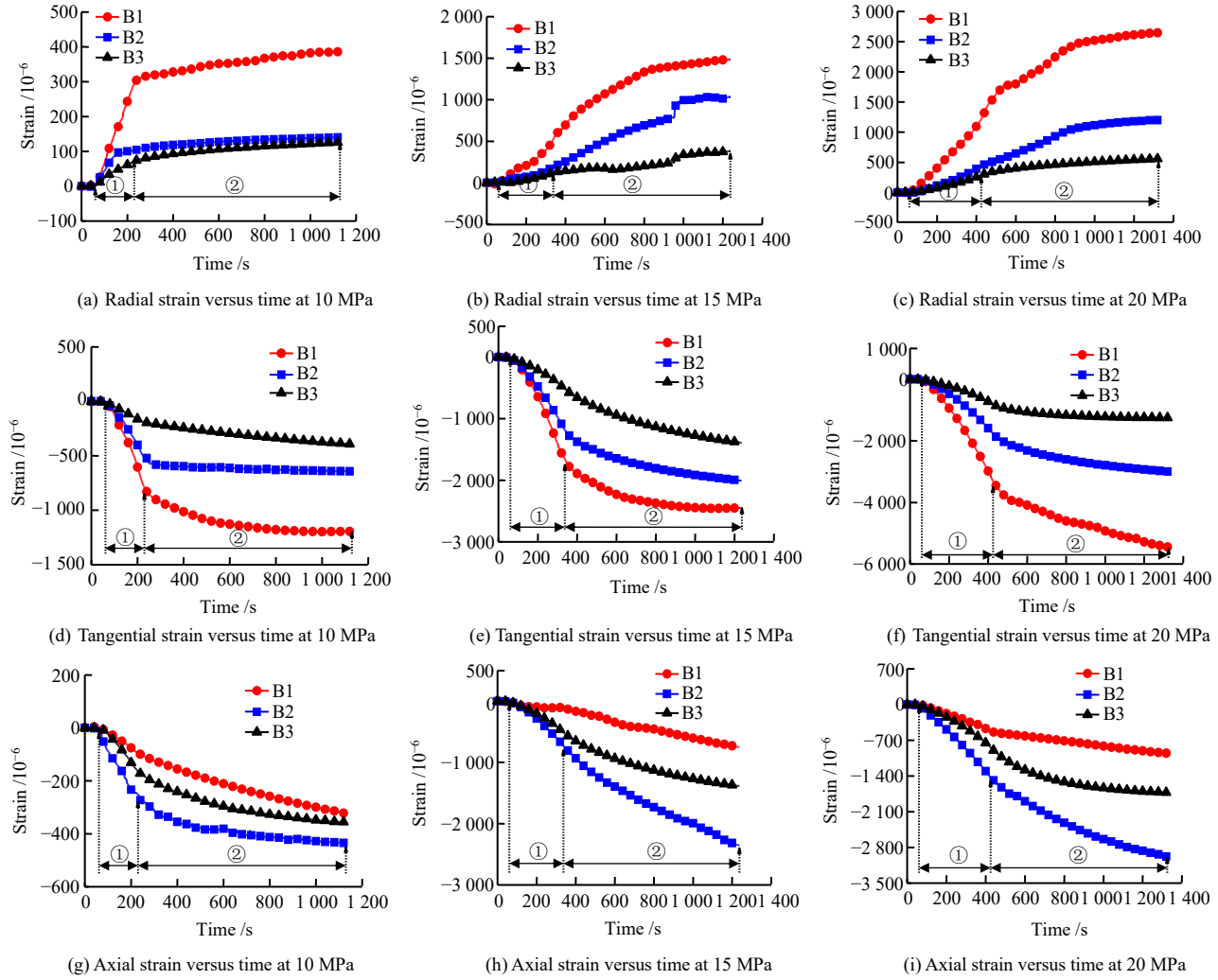

(a) Radial strain versus time at 10 MPa (b) Radial strain versus time at 15 MPa (c) Radial strain versus time at 20 MPa

(d) Tangential strain versus time at 10 MPa (e) Tangential strain versus time at 15 MPa (f) Tangential strain versus time at 20 MPa

(g) Axial strain versus time at 10 MPa (h) Axial strain versus time at 15 MPa (i) Axial strain versus time at 20 MPa

Note: ① denotes the unloading stage; ② denotes the post-unloading maintenance stage.

Fig. 6 Strain characteristics of surrounding rock at the corner

point, and a compressive strain peak exists inside the surrounding rock.

3.1.3 Analysis of comprehensive strain characteristics and mechanism of roadway surrounding rock

The deformation characteristics of the surrounding rock specimens under different initial in-situ stresses are similar. We take the strain characteristics of the measurement points in surrounding rock specimens under 15 MPa as an example to examine the variation of surrounding rock deformation at the roof and corner with radius, as shown in Fig.7. Where r is the distance from the measuring point to the center of the roadway; and R_0 is the radius of the chamber (R_0 = 20 mm for the surrounding rock specimen).

The analysis shows that, the roadway tensile deformation is dominated by the radial tension of the surrounding rock at the roof and side-wall, as well as the tangential compressive deformation of the corner wall rock. It is also found that there is a critical zero point of tension and compression for the tangential strain of

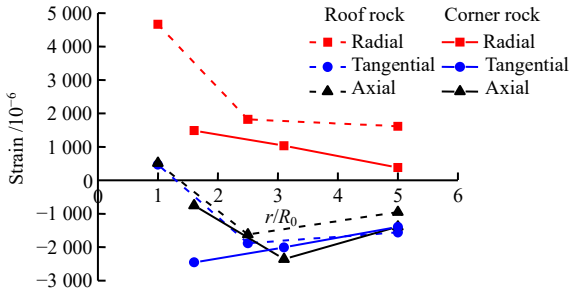

Fig. 7 Strain evolution of the roof and corner with depth

the surrounding rock at the roof (side-wall) in the area of 1 to 2.5 times the excavation radius, and all the corner rock is tangentially compressed. That is, during the excavation and unloading process, a symmetrical neutral layer of tangential strain is formed around the central axis of the surrounding rock of the roof (side-wall) and extends to the corner surrounding rock, with the inner side being the tension zone and outer side being the compression zone. This strain characteristic is consistent with the deformation of coal roadway studied by previous research[18].

3.2 Stress-strain characteristics around the roadway under different initial geostresses

In actual engineering, the rectangular roadway is mainly concerned about the damage and deformation around the roadway. Therefore, this paper takes the measurements at points A1(roof rock) and B1 (corner rock) to produce deviatoric stress−strain curves around the roof and corner wall rock under different initial geostresses, as shown in Fig.8. Comparative analysis of the test results shows that:

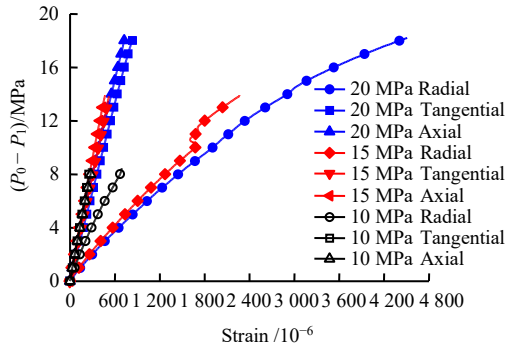

(a) Deviatoric stress−strain curves of roof rock

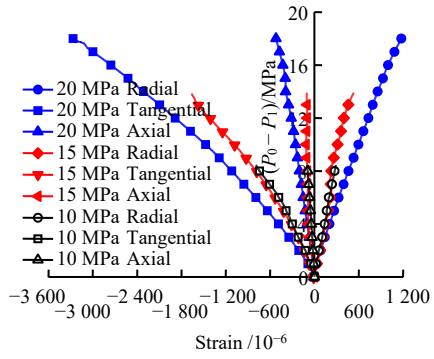

(b) Deviatoric stress−strain curves of corner rock

Fig. 8 Deformation characteristics of surrounding rock around roadway under different initial geostresses

(1) The three-dimensional strain laws around the roadway are the same, that is, the magnitude of in-situ stress has no effect on the tension and compression of the surrounding rock.

(2) For roof rock, the radial strain plays a leading role. When the in-situ stress increases from 10 MPa to 15 MPa, the radial deformation rate is significantly accelerated, while when the in-situ stress increases from 15 MPa to 20 MPa, there is insignificant growth in the radial deformation rate. The increase of in-situ stress has little effect on the axial and tangential deformation.

(3) For the corner wall rock, the tangential strain plays a leading role. When the in-situ stress increases from 10 MPa to 15 MPa, the tangential deformation rate is almost unchanged, while when the in-situ stress increases from 15 MPa to 20 MPa, the tangential deformation rate is significantly accelerated. Again, the increase of in-situ stress has little effect on axial and tangential deformation.

To sum up, the influence mechanism of the initial in-situ stresses on the surrounding strain of roadway is concluded as follows:

(1) According to the strain evolution characteristics discussed in Section 3.1, with the removal of the internal confining pressure, the surrounding rock moves towards the center of the roadway. The contact effect of the roof and the wall weakens the radial deformation of the corner wall rock and transforms it into tangential compressive deformation. Therefore, under different initial stresses, the radial deformation of the roof (side-wall) and the tangential deformation of the corner are predominantly responsible for the damage and destruction of surrounding rock around the road-way.

(2) From a mesoscopic perspective of micro-crack propagation inside the surrounding rock of the roadway[19], the changes of stress would cause tensile (compressive) stress concentration at the crack tip during the excavation and unloading process. When the stress is greater than the critical failure strength, microcracks propagate and cause deformation in the surrounding rocks. According to the internal failure characteristics of the test specimens (see Fig.11) and the mechanical properties of cement mortar, strong in compression and weak in tension, the following deductions are made: when the initial in-situ stress is 10 MPa, the magnitude of the in-situ stress is small, and there is no obvious internal rock failure with insignificant micro-crack propagation, so the rates of tangential deformation in the roof and radial deformation in the corner are both low. When the initial in-situ stress is 15 MPa, the change of stress results in a large number of tensile cracks in the roof with the deformation rate increases rapidly. The material compression resistance allows the corner rock to maintain a low deformation rate. When the initial in-situ stress increases to 20 MPa, the deformation rate of the corner rock rapidly increases due to the high geostress.

4 AE characteristics and analysis

4.1 AE time domain characteristics

The AE impact count characterizes the initial initiation and propagation of internal cracks of the specimen[20], reflecting changes in the number of cracks. According to Eq.(1), the damage evolution characteristics of surrounding rock specimens over time can be determined[21].

$$D_{SB} = \Omega / \Omega_m \tag{1}$$

where Ω is the cumulative impact count (or energy) of the AE of the specimen since the beginning of loading to any time before the end of test; Ω_m is the cumulative impact count (or energy) for the entire test process; and D_{SB} is the relative damage of the surrounding rock specimen at that time. This paper uses the AE impact count as a statistical object.

Figure 9 shows the evolution of the AE impact count rate and damage variable D_{SB} of the surrounding rock specimens over time. It can be seen that although the initial in-situ stress is different, a periodic trend is observed for the entire test process with characteristics and analysis as follows:

(1) Loading and post-loading maintenance phases: As loading continues, the AE impact count rate gradually increases and reaches a peak, corresponding to 3.3×10^4, 6.2×10^4, 8.1×10^4, 1.9×10^5 in sequence. After entering the maintenance phase, the AE impact count rate gradually decreases, and the growth rate of damage variable D_{SB} gradually stabilizes.

(2) Unloading phrase: In the early stage of unloading, the impact count rate is relatively low. As unloading continues, the internal energy of the test specimen accumulates, and the impact count rate starts to rise and the D_{SB} increases rapidly, indicating that internal cracks in the test specimen have begun to emerge and expand. In the later period, the impact count rate gradually reaches a peak corresponding to the completion of the main fracture.

(3) During the post-unloading maintenance phase, the AE impact count rate gradually stabilizes; the growth rate of the damage variable D_{SB} tends to be flattened. The higher the in-situ stress, the longer the effect of unloading lasts on the internal rock, the more active is the impact count rate, and the greater is the relative damage proportion.

According to the time domain characteristics of AE under different geostress levels, it is concluded that,

(1) Under in-situ stresses of 10 and 15 MPa, the peak points of the impact count rate occur at 3.35 MPa and 1.3 MPa in the unloading stage, respectively; under the in-situ stress of 20 MPa, the peak point of the impact count rate appears at 57 s after unloading. This means

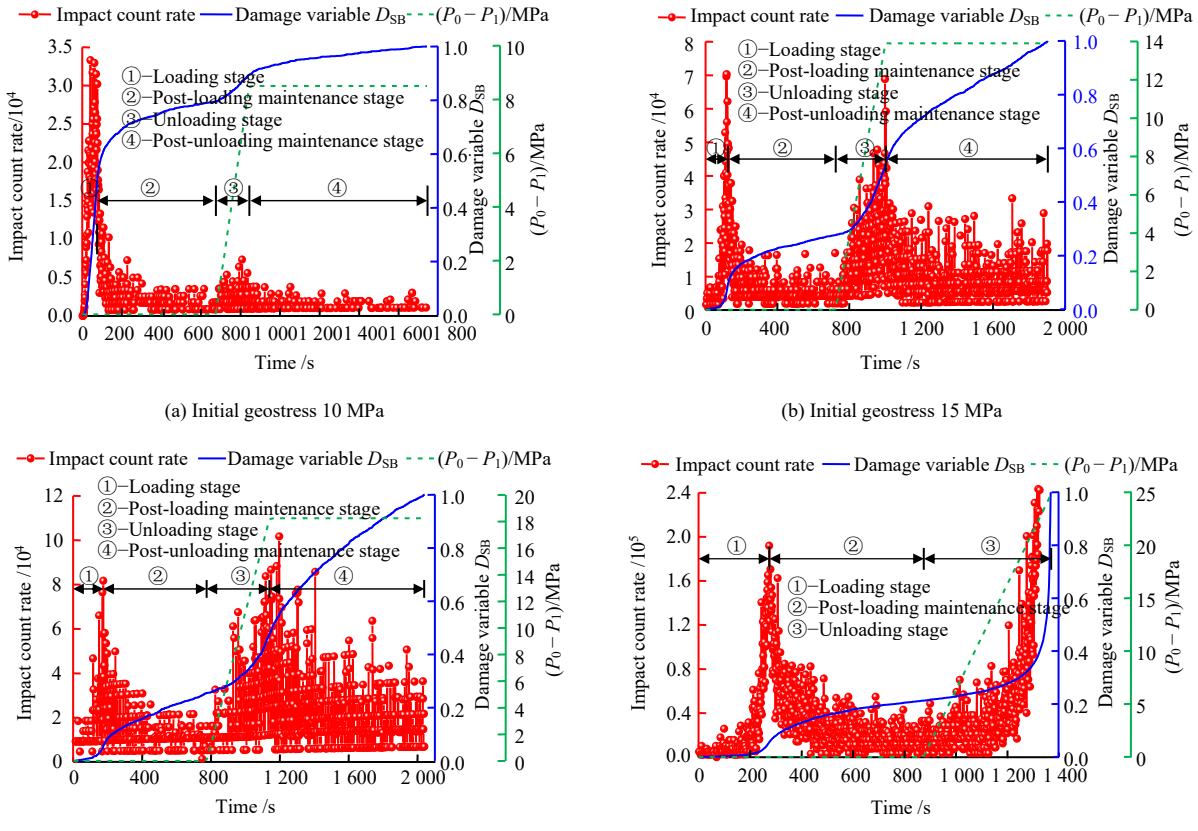

(a) Initial geostress 10 MPa

(b) Initial geostress 15 MPa

(c) Initial geostress 20 MPa

(d) Initial geostress 30 MPa

Fig. 9 Evolution characteristics of AE time domain under different initial geostresses

that given the surrounding-rock specimen still has bearing capacity after excavation unloading, the higher the geostress, the more relative delay in the time for the main fracture to occur, even until within a period of time after the unloading is completed.

(2) The damage variable D_{SB} is a relative value based on the overall damage of the surrounding rock specimen. The relative damage D_{SB} after unloading is 20.5%, 72.3%, 74.5%, and 78.8% in sequence that increase nonlinearly with the increase of the initial geostress.

4.2 AE frequency domain characteristics

Fast Fourier transform (FFT) was performed on the AE waveform data obtained from the unloading and post-unloading maintenance phases to acquire the peak frequency−time−amplitude evolution relationship, as shown in Fig.10, which can intuitively display the

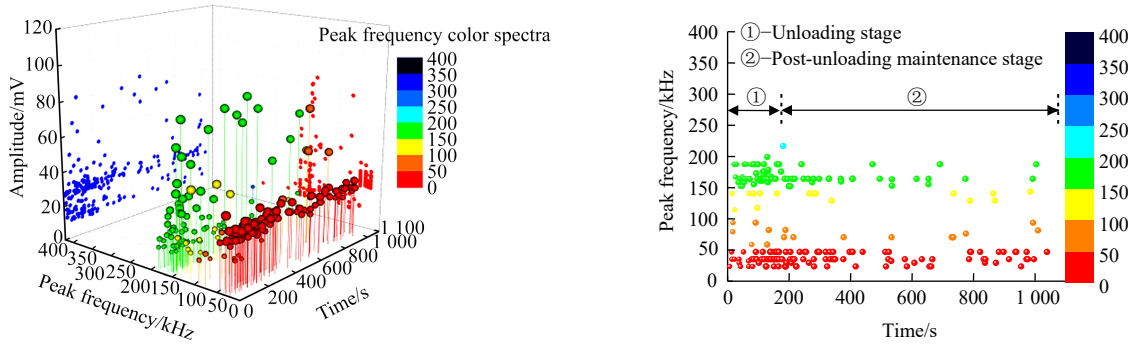

(a) AE peak frequency−amplitude−time evolution relationship at initial geostress of 10 MPa

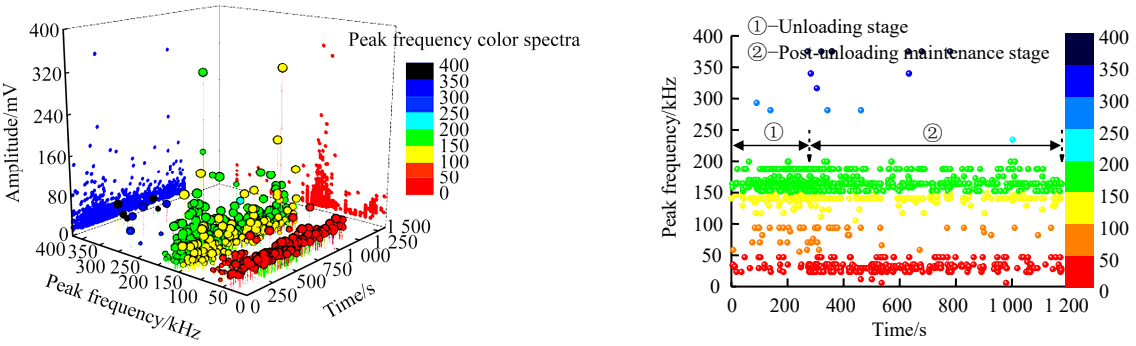

(b) AE peak frequency−amplitude−time evolution relationship at initial geostress of 15 MPa

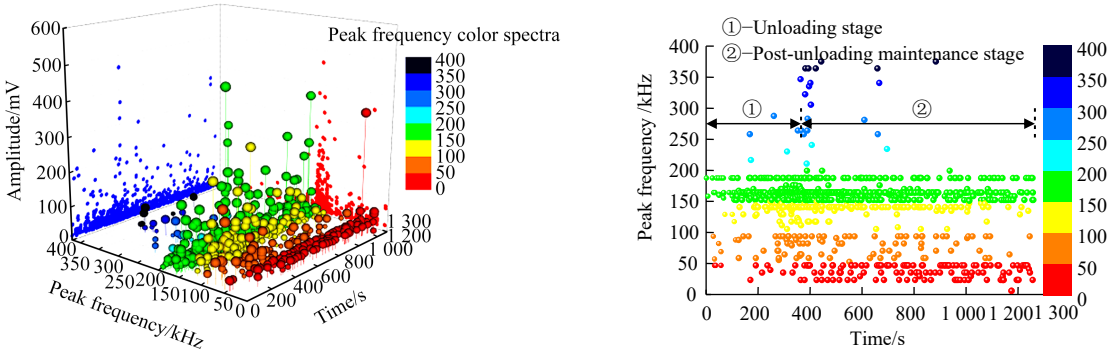

(c) AE peak frequency−amplitude−time evolution relationship at initial geostress of 20 MPa AE

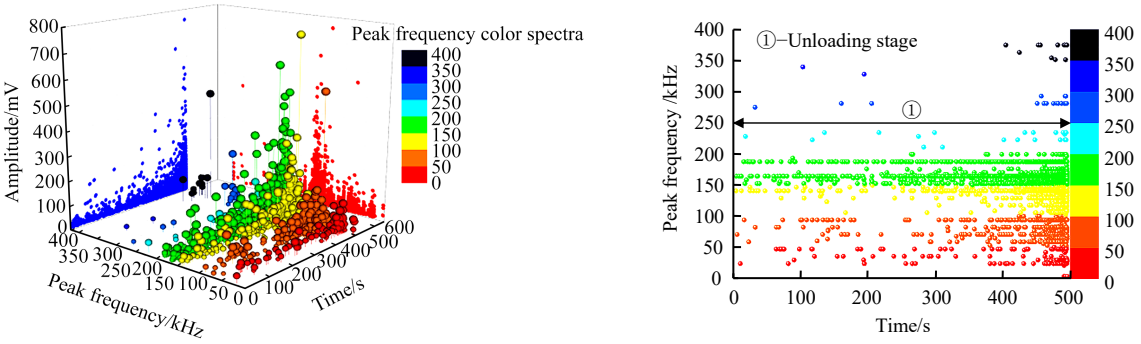

(d) AE peak frequency−amplitude−time evolution relationship at initial geostress of 30 MPa

Fig. 10 Evolution characteristics of AE frequency domain under different initial geostresses

active degree of AE signal and peak frequency characteristics.

(1) When the initial geostress is 10 MPa, the numbers of AE events are low, as shown in Fig.10(a). In the early stage of unloading, the peak frequencies distribution are relatively scattered, and the AE amplitudes are low. Subsequently, the numbers of AE events increase and are mainly distributed in two frequency bands of 20−50, 160−180 kHz, and the amplitudes of AE gradually increase until reaching the peak. In the post-unloading maintenance phase, the peak-frequency signals are relatively scattered.

(2) The frequency characteristics of the initial geostress of 15 MPa and 20 MPa are similar to each other, and the numbers of AE events increase significantly, as shown in Figs. 10(b) and 10(c). In the early stage of unloading, the peak frequencies are concentrated in the 150−170 kHz band. As unloading continues, the peak frequency signals start to increase while the AE amplitudes gradually increase as well. Before the main fracture of the surrounding rock specimen, the peak-frequency signals are concentrated in the 20−45, 80−95, 140−180 kHz frequency bands, and the high peak frequency signals appear at the same time; the frequency band interval becomes wider, and the AE amplitudes reaches the peak. In the post-unloading maintenance phase, the peak frequency signals decrease relatively, and the distribution regions gradually stabilize.

(3) When the initial ground stress is 30 MPa, the AE signals increase with the appearance of the higher peak frequency; the AE amplitude gradually increases and the trend change is observed. In the early stage when the surrounding rock specimen loses its bearing capacity, the peak frequencies occupy the 20−180 kHz frequency band. Meanwhile, the AE amplitude gradually reaches its peak with the peak frequency signals.

Combining the peak frequency evolution characteristics under different initial geostresses, it can be seen that in the initial stage of unloading, the peak frequency signal distribution is relatively dispersed; it gradually becomes relatively concentrated when the unloading reaches a certain point, and the higher the initial ground stress, the more the number of concentrated distribution band; the peak-frequency signals reach the widest distribution at the moment when the main fracture occurs in the surrounding rock specimen; the higher amplitude signals also appear in the post-unloading maintenance stage, which may be caused due to micro-cracks growing to macro-cracks by secondary stress adjustment.

Previous research has also observed similar phenomenon in the triaxial tests of rock materials[22−23], and the amplitude of the acoustic emission signal gradually increases around 180 kHz when the granite is about to be destroyed. Our roadway excavation unloading model tests once again provide similar evidence. Therefore, the phenomenon of increasing range of AE signal peak frequency and gradual increase of signal amplitude is regarded as a precursor information of main fracture occurring in the surrounding rock.

5 Failure characteristics and mechanism analysis

The failure characteristics of the surrounding rock specimens after excavation and unloading under different initial geostresses are illustrated in Fig.11. The figure shows:

(1) When the local stress level is 10 MPa, there is no obvious damage, however, there appear some micro-cracks on the inner wall of the roadway.

(2) When the local stress level is 15 MPa, annular cracks appear on the outer wall, and the inner wall is observed with stratification; transverse cracks appear on the roof and side-wall surface with obvious heaving and cracking; the damage to the corner wall rock is comparatively insignificant.

(3) When the local stress level is 20 MPa, annular cracks also appear on the outer wall, with heaving on the roof and side-wall accompanied by severely layered and massive spalling.

(4) When the local stress level is 30 MPa, the specimen loses its load-bearing capacity in the later stage of unloading and eventually broke; an obvious compression-shearing annular failure zone appears at the cross-section of 1/3 height of the outer wall with axial splitting. Severe tensile swelling and spalling occur at the roof and side of the inner wall, and the corner surrounding rock is accompanied by compression and shear failure.

The analysis shows that, the free face formation due to the excavation unloading of the roadway causes the redistribution of stress in the surrounding rock, and the influence of the stress redistribution on the instability of the surrounding rock depends on the initial in-situ stress; the failure mode of a rectangular roadway is mainly concerned about the tensile heaving, accompanied by the delamination phenomenon, at the roof and sidewall. The corner wall rock does not show obvious compression-shear failure until the specimen loses its load-bearing capacity. This failure phenomenon is similar to the type of surrounding rock failure in actual engineering sites[24], and is consistent with the

(a) Initial geostress 10 MPa (b) Initial geostress 15 MPa (c) Initial geostress 20 MPa (d) Initial geostress 30 MPa

Fig. 11 Failure characteristics of specimens

mechanical theory studied by previous research[17].

The failure mechanism is that, during the unloading process, when the local stress is sufficiently high and the span of the roadway is sufficiently large, the mechanical properties of the rectangular structure cause the tensile stress to concentrate in the middle. As delamination cracks continue to develop, the contact effect of the roof- and the side wall-rock at the corners causes the corner wall rock to be compressed, so the most serious damage occurs at the roof and side wall. When the surrounding rock specimen is under a high in-situ stress, the delamination tensile cracks extend to deeper part of the surrounding rock, and eventually form a transverse crack through a weak section. Subsequently, the surrounding rock specimen loses its bearing capacity and overall failure occurs.

According to the deformation and failure characteristics of the surrounding rock specimens, the following points should be noted in the excavation of deep-buried rectangular roadways under high in-situ stresses: (i) The form of supporting while excavating or supporting in advance should be adopted to suppress the initiation and expansion of delamination cracks ahead of time. (ii) Targeted reinforcement control should be implemented at the maximum deformation and the main extension range of the delamination. (iii) The characteristics of the stability of surrounding rocks at depth should be leveraged in combination with a variety of supporting forms to reduce the impact of excavation unloading.

6 Conclusion

The roof and the two sides are mainly deformed by radial tension; from the periphery of the roadway towards deep surrounding rock, the tangential and axial strains change from tension to compression. The corner rock is mainly deformed under tangential compression, and tensile and compressive strain characteristics are exhibited in the radial and axial directions, respectively. The radial strain rate of the roof (side-wall) and the tangential strain rate of the corner surrounding rock are significantly affected by the stress level of the ground.

Under the premise that the surrounding rock specimen still has bearing capacity after excavation and unloading, the higher the ground stress, the time for the main fracture to occur will be relatively delayed, even within a period of time after the unloading is completed. The relative damage ratio of the surrounding rock specimens after excavation and unloading shows a non-linear increase with the increase of the ground stress level.

The phenomenon of an increasing number of the concentrated regions of AE signal peak frequency and the gradual increase of AE signal amplitude can be regarded as a precursor information of the upcoming main fracture in the surrounding rock. The higher the initial geostress, the wider the peak frequency signal distribution in the early stage of the main fracture.

The inner wall of the surrounding rock specimen under different magnitudes of in-situ stress after excavation unloading shows the evolution process from microcrack, stratified cracking and heaving to massive spalling. The failure of rectangular roadway is mainly characterized by the tensile uplift of roof and surrounding rock, accompanied by the phenomenon of stratified cracking and bulging. When the bearing capacity of the specimens is lost, the corner surrounding rock shows the characteristics of compression-shear failure.

References

[1] JIN C Y, YANG C X, FANG D, et al. Study on the failure mechanism of basalts with columnar joints in the unloading process on the basis of an experimental cavity[J]. Rock Mechanics and Rock Engineering, 2015, 48(3): 1275−1288.

[2] GAO F Q, STEAD D, KANG H P. Numerical simulation of squeezing failure in a coal mine roadway due to mining–induced stresses[J]. Rock Mechanics and Rock Engineering, 2015, 48(4): 1635−1645.

[3] QIU Shi-li, FENG Xia-ting, ZHANG Chuan-qing, et al. Experimental research on mechanical properties of deep-buried marble under different unloading rates of confining pressures[J]. Chinese Journal of Rock Mechanics and Engineering, 2010, 29(9): 1807−1817.

[4] HUANG Run-qiu, HUANG Da. Experimental research on affection laws of unloading rates on mechanical properties of Jinping marble under high geostress[J]. Chinese Journal of Rock Mechanics and Engineering, 2010, 29(1): 21−33.

[5] LI X B, DU K, LI D Y. True triaxial strength and failure modes of cubic rock specimens with unloading the minor principal stress[J]. Rock Mechanics and Rock Engineering, 2015, 48(6): 2185−2196.

[6] SU G S, JIANG J Q, ZHAI S B, et al. Influence of tunnel axis stress on strain burst: an experimental study[J]. Rock Mechanics and Rock Engineering, 2017, 50(6): 1551−1567.

[7] DU K, TAO M, LI X B, et al. Experimental study of slabbing and rockburst induced by true-triaxial unloading and local dynamic disturbance[J]. Rock Mechanics and Rock Engineering, 2016, 49(9): 3437−3453.

[8] LI X B, FENG F, LI D Y, et al. Failure characteristics of granite influenced by sample height-to-width ratios and intermediate principal stress under true-triaxial unloading conditions[J]. Rock Mechanics and Rock Engineering, 2018, 51(5): 1321−1345.

[9] THOMAS BRUNING, MURAT KARAKUS, GIANG D NGUYEN, et al. Experimental study on the damage evolution of brittle rock under triaxial confinement with full circumferential strain control[J]. Rock Mechanics and Rock Engineering, 2018, 51(11): 3321−3341.

[10] HOU Gong-yu, NIU Xiao-song. Perfect elastoplastic solution of axisymmetric circular openings in rock mass based on Levy-Mises constitutive relation and D-P yield criterion[J]. Rock and Soil Mechanics, 2009, 30(6): 1555−1562.

[11] HOU Gong-yu, LI Xiao-rui, LIANG Hong-yao, et al. Study on deformation and failure of high-strength gypsum surrounding rock specimens (thick-walled cylinder) simulating roadway excavation[J]. Journal of China Coal Society, 2018, 43(3): 616−625.

[12] WANG Meng, NIU Yu-he, YU Yong-jiang, et al. Experimental research on characteristics of deformation and failure of surrounding rock of roadway in deep mine under influence of principal stress evolution[J]. Chinese Journal of Geotechnical Engineering, 2016, 38(2): 237−244.

[13] YANG S Q. Experimental study on deformation, peak strength and crack damage behavior of hollow sandstone under conventional triaxial compression[J]. Engineering Geology, 2016, 213(4): 11−24.

[14] WANG S F, LI X B, DU K, et al. Experimental study of the triaxial strength properties of hollow cylindrical granite specimens under coupled external and internal confining stresses[J]. Rock Mechanics and Rock Engineering, 2018, 51(7): 2015−2031.

[15] HOU Gong-yu, LI Xiao-rui, ZHANG Zhen-duo, et al. Experimental system for simulating excavation unloading process of rock around roadway by using small cylindrical hollow specimen[J]. Chinese Journal of Rock Mechanics and Engineering, 2017, 36(9): 2136−2145.

[16] HOU Gong-yu, JING Hao-yong, LIANG Jin-ping, et al. Experimental study of deformation and acoustic emission characteristics of rectangular roadway under different unloading rates[J]. Rock and Soil Mechanics, 2019, 40(9): 3309−3318.

[17] XU Shuan-qiang, YU Mao-hong, HU Xiao-rong. Study on stability of underground circular cavern based on double shear unified strength theory[J]. Journal of China Coal Society, 2003, 28(5): 522−526.

[18] HE Man-chao, ZHANG Guo-feng, WANG Gui-lian, et al. Research on mechanism and application to floor heave control of gateway[J]. Chinese Journal of Rock Mechanics and Engineering, 2009, 28(Suppl.1): 2593−2598.

[19] CHEN Wei-zhong, LÜ Sen-peng, GUO Xiao-hong, et al. Unloading confining pressure for brittle rock and mechanism of rock burst[J]. Chinese Journal of Geotechnical Engineering, 2010, 32(6): 963−969.

[20] ZHAO Xing-dong, TANG Chun-an, LI Yuan-hui, et al. Study on an activity characteristics under uniaxial compression loading[J]. Chinese Journal of Rock Mechanics and Engineering, 2016, 25(2): 3673−3678.

[21] SELAHATTIN AKDAG, MURAT KARAKUS, ABBAS TAHERI, et al. Effects of thermal damage on strain burst mechanism for brittle rocks under true-triaxial loading conditions[J]. Rock Mechanics and Rock Engineering, 2018, 51(6): 1657−1682.

[22] JI Hong-guang, LU Xiang. Characteristics of acoustic emission and rock fracture precursors of granite under conventional triaxial compression[J]. Chinese Journal of Rock Mechanics and Engineering, 2015, 34(4): 694−702.

[23] MIAO Jin-li, HE Man-chao, LI De-jian, et al. Acoustic emission characteristics of granite under strain rockburst test and its micro-fracture mechanism[J]. Chinese Journal of Rock Mechanics and Engineering, 2009, 28(8): 1593−1603.

[24] LI Wei-teng, LI Shu-cai, WANG Qi, et al. Model test study of surrounding rock deformation and failure mechanism of deep roadway with thick top coal[J]. Rock and Soil Mechanics, 2013, 34(10): 2847−2856.